Journal of Solid State Chemistry 183 (2010) 1767–1775

Contents lists available at ScienceDirect

Journal of Solid State Chemistry

journal homepage: www.elsevier.com/locate/jssc

Intermetallic and metal-rich phases in the system Li–Ba–In–N

Volodymyr Smetana [a], Grigori V. Vajenine [a,b], Lorenz Kienle [c], Viola Duppel [a], Arndt Simon [a,*]

[a] Max-Planck-Institut für Festkörperforschung, Heisenbergstraße 1, D-70569 Stuttgart, Germany
[b] Institut für Anorganische Chemie, Universität Stuttgart, Pfaffenwaldring 55, D-70569 Stuttgart, Germany
[c] Institut für Materialwissenschaft, Christian-Albrechts-Universität zu Kiel, Kaiserstraße 2, D-24143 Kiel, Germany

ARTICLE INFO

Article history:
Received 6 April 2010
Received in revised form
19 May 2010
Accepted 19 May 2010
Available online 27 May 2010

Keywords:
Subvalent compounds
Intermetallic phases
Nitrides
Lithium
Indium
Barium

ABSTRACT

Three new intermetallic phases, $BaLi_{2.1}In_{1.9}$, $BaLi_{1.12}In_{0.98}$, and $BaLi_{1.06}In_{1.16}$ and two subnitrides $Li_{35}In_{45}Ba_{39}N_9$ and $LiIn_2Ba_3N_{0.83}$ have been synthesized and their crystal structures have been determined. According to single crystal X-ray diffraction data $BaLi_{2.1}In_{1.9}$ and $BaLi_{1.12}In_{0.98}$ crystallize with hexagonal symmetry ($BaLi_{2.1}In_{1.9}$: $P6_3/mmc$, $a=10.410(2)$, $c=8.364(2)$ Å, $Z=6$, $V=785.0(2)$ Å^3) and $BaLi_{1.12}In_{0.98}$: $P6/mmm$, $a=17.469(1)$, $c=10.6409(7)$ Å, $Z=30$, $V=2813.5(8)$ Å^3), while $BaLi_{1.06}In_{1.16}$ has a rhombohedral structure (R-3c, $a=18.894(3)$, $c=85.289(17)$ Å, $Z=276$, $V=26368(8)$ Å^3). $BaLi_{2.1}In_{1.9}$ is isostructural with the known phase $BaLi_4$. The phase $BaLi_{1.12}In_{0.98}$ is structurally related to $Na_8K_{23}Cd_{12}In_{48}$, while $BaLi_{1.06}In_{1.16}$ is isostructural with $Li_{33.3}Ba_{13.1}Ca_3$. A sample containing structurally similar $BaLi_{1.12}In_{0.98}$ and $BaLi_{1.02}In_{1.16}$ was also investigated by transmission electron microscopy. $Li_{35}In_{45}Ba_{39}N_9$ and $LiIn_2Ba_3N_{0.83}$ crystallize with tetragonal (I-42m, $a=15.299(2)$, $c=30.682(6)$ Å, $Z=2$, $V=7182(2)$ Å^3) and cubic (Fd-3m, $a=14.913(2)$ Å, $Z=8$, $V=3316.7(7)$ Å^3) symmetry, respectively. While the first-mentioned subnitride belongs to the $Li_{80}Ba_{39}N_9$ structure type, the second extends the structural family of $Ba_6In_{4.78}N_{2.72}$. The structural features of the new compounds are discussed in comparison to the known phases and the results of total energy calculations.

1. Introduction

The interplay between the classical bonding modi such as ionic, metallic, and covalent in solid-state materials is of fundamental interest both for the improvement of synthesis planning and for understanding the product properties. Metal-rich compounds of electropositive elements offer a fruitful playground for such investigations. So, a large number of metal-rich nitrides of sodium in combination with barium have been discovered [1]. All these compounds can be grouped into a family with a common structural feature. They exhibit ionic bonding between barium and nitrogen atoms in one part of the structure resulting in discrete or condensed ionic clusters and metallic bonding in the surrounding. No Na–N bonding contacts have been observed. The situation has been changed drastically with the introduction of lithium. This element was found to play an important role both in the metallic region and in the nitride clusters [2–5]. Several ternary intermetallic compounds with lithium have also been discovered, namely $Li_{13}Na_{29}Ba_{19}$, $Li_{33.3}Ba_{13.1}Ca_3$, and $Li_{18.9}Na_{8.3}Ba_{15.3}$ [6,7], which contain a novel structural feature, homoatomic centered (poly-) icosahedral lithium clusters.

Many metal-rich alkaline-earths containing nitrides have been reported with triels, especially Ga and In [8–14]. In all these compounds there is also insufficient nitrogen content for full oxidation of the metals. However, the formal oxidation state of indium is negative and indium–indium bonding is common. Moreover, two phases with the general composition $Ae_6In_4(In_xLi_y)N_{3-z}$ (Ae=Sr or Ba) [15] have been observed. In the strontium-containing phase in addition to In_4 and Sr–N clusters also positions with mixed occupation by Li and In are present, in spite of the chemical difference between these elements. Binary systems of triels and alkaline-earth or alkali metals have been intensively investigated and a large number of binary phases have been reported. Four compounds are known in the system Li–In (LiIn, $Li_{13}In_3$, Li_2In, and Li_3In_2 [16,17]), seven in the system Sr–In ($SrIn_4$, $SrIn_2$, Sr_3In_{11}, SrIn, $Sr_{11}In_7$, Sr_5In_3, and $Sr_{2.33}In_{0.92}$ [18–22]) and five in the system Ba–In ($BaIn_4$, $BaIn_2$, BaIn, Ba_2In, and Ba_3In [20,22,23]), however, the existence of the latter two has not been confirmed by structural investigations. Ba_2In is described as existing in a low- and high-temperature modification, α- and β-Ba_2In, respectively. According to a recent investigation [24], "α-Ba_2In" actually has the composition Ba_9In_4.

Introducing the In component into the investigation of new quaternary subnitrides seemed to be a promising step. On one

* Corresponding author. Fax: +49 711 689 1642.
E-mail address: A.Simon@fkf.mpg.de (A. Simon).

0022-4596/$ - see front matter © 2010 Elsevier Inc. All rights reserved.
doi:10.1016/j.jssc.2010.05.021

side, indium might play the role of the monovalent analogue of the alkali metals, much like thallium does. On the other side, the typical p-block chemical properties such as a tendency towards covalent bonding might play a role. The possibility of a substitution of the lightest alkali metal lithium by heavy indium is particularly of interest. In this work, we report on the synthesis and crystal structure investigations of three new Li–In–Ba intermetallic phases and two subnitrides in the system Li–In–Ba–N. Their structures are discussed and compared with those of known phases and with the results of total energy calculations.

2. Experimental

2.1. Reagents

Ba metal (Merck, 99%, distilled twice with an intermediate heating in a closed tantalum container at 1200 K in vacuum in order to remove hydrogen), Li metal (Merck, 99%), In metal (Merck, 99,99%), $Ba(N_3)_2$ (Schuchardt, 98.5%, recrystallized and dried under vacuum), and NaN_3 (Merck 99.9%) were used for syntheses.

2.2. Syntheses

Due to the extreme sensitivity of some educts and the products to air, all handling was performed under purified argon using the Schlenk technique or a glove box. Reactions were performed in closed tantalum containers which were arc-welded and sealed inside Pyrex glass ampoules. *$BaLi_{2.1}In_{1.9}$*: Two samples were prepared with the overall stoichiometry $BaLi_2In_2$ (200 mg Ba, 334.4 mg In, and 20.4 mg Li). *$BaLi_{1.12}In_{0.98}$*: The sample with the intended composition Li_2InBa (400 mg Ba, 334.3 mg In, and 40.8 mg Li) resulted in a single-phase product judged from X-ray investigation of single crystals, the excess of Li being not visible in the powder diagram. An attempt to obtain $BaLi_{1.12}In_{0.98}$ from the stoichiometric reaction mixture resulted in a high yield product, however, with not yet fully unidentified impurities. Single crystals of $BaLi_{1.06}In_{1.16}$ were first obtained in an intended synthesis of $BaLi_{1.12}In_{0.98}$. A stoichiometric sample (300 mg Ba, 291 mg In, and 16.2 mg Li) resulted also in a high yield of $BaLi_{1.06}In_{1.16}$ with $BaLi_{1.12}In_{0.98}$ as a main impurity. *$Li_{35}In_{45}Ba_{39}N_9$:* A sample (300 mg Ba, 257.2 mg In, 23.5 mg Li, and 10.9 mg NaN_3) with the overall composition $3Na+20Li+Li_{40}In_{40}Ba_{39}N_9$ was prepared in order to obtain the compound isostructural with $Li_{80}Ba_{39}N_9$, yielding single crystals of the new subnitride. *$LiIn_2Ba_3N_{0.83}$*: A sample with the stoichiometric composition $LiIn_2Ba_3N$ (472.2 mg Ba, 278.6 mg In, 8.5 mg Li, and 44.8 mg BaN_6) resulted in a high yield product. In order to obtain single crystals of better quality another sample with a 50% lithium excess was prepared.

All samples were heated to 650 °C and annealed at this temperature for 50 h, followed by cooling to 350 °C at a rate of 1 °C h^{-1}, further annealing for 1 month, and cooling to room temperature at a rate of 3 °C h^{-1}.

2.3. Determination of crystal structure

Powder diffraction diagrams were measured for all samples after grinding and sealing them in glass capillaries under argon atmosphere. The diffraction data were collected on a STOE STADI-P diffractometer with MoK_α radiation. Single crystals were sealed under argon atmosphere in glass capillaries for X-ray investigations. Diffraction data were collected at room temperature using a STOE IPDS II diffractometer with monochromatized MoK_α radiation by oscillating the crystals around the ω axis. The starting atomic parameters derived via direct methods using the program SIR 97 [25] were subsequently refined with the program SHELX-97 [26] (full-matrix least-squares on F^2) within the WinGX program package [27]. The positions of the Li atoms were found in difference Fourier maps with reasonable interatomic distances as the main criterion. Further details of the crystal structure investigations may be obtained from Fachinformationszentrum Karlsruhe, 76344 Eggenstein-Leopoldshafen, Germany (fax: (+49)7247-808-666; e-mail: crysdata@fiz-karlsruhe.de, http://www.fiz-karlsruhe.de/request_for_deposited_data.html) on quoting the respective CSD numbers 421540 ($BaLi_{1.02}In_{1.08}$), 421541 ($BaLi_{1.06}In_{1.16}$), 421542 ($BaLi_{1.12}In_{0.98}$), 421543 ($BaLi_{2.1}In_{1.9}$), 421544 ($Li_{35}In_{45}Ba_{39}N_9$), and 421545 ($LiIn_2Ba_3N_{0.83}$).

2.4. Electron microscopy

HRTEM (high-resolution transmission electron microscopy), SAED (selected area electron diffraction) and PED (precession electron diffraction) were performed with an electron microscope CM 30 ST (Philips, LaB_6 cathode, accelerating voltage: 300 kV), equipped with an EDX system (Noran Company, Vantage System) [28–32]. The image was recorded with a multiscan CCD camera (Gatan). Because of extreme air and moisture sensitivity of the samples all manipulations for the preparation and transfer were carried out under dry argon with the aid of a special device [33,34]. A perforated carbon/copper net served as support for the crystallites. Using the PED (“spinning star” by Nano-MEGAS, precession angle: 3°) the multiple scattering could be reduced to a minimum. Simulations of HRTEM images (multislice formalism [35,36]) and of SAED patterns (kinematical approximation) were calculated with the EMS program package [37]. The software Emaps was used to simulate PED diagrams [38]. All images were recorded with a Gatan Multiscan CCD camera and evaluated (including Fourier filtering) with the program Digital Micrograph 3.6.1 (Gatan). All HRTEM images were filtered after Fourier transformation by using a suitable band-pass mask. Fourier transformations of high-resolution images were calculated with the program CRISP [39].

2.5. Elemental analysis

The chemical compositions of the products were determined by energy-dispersive X-ray analysis (EDX) performed on a Tescan 5130 MM scanning electron microscope (SEM) equipped with an Oxford EDX detector. Selected crystals were fixed on the SEM sample holder using carbon tape. Data were collected by applying a 20 kV accelerating voltage with an accumulation time of 60–90 s. According to EDX investigations, the atomic ratio of Ba and In in $BaLi_{1.12}In_{0.98}$ (Ba:In from 1.1:1 to 0.92:1) and $BaLi_{2.1}In_{1.9}$ (Ba:In from 0.55:1 to 0.54:1) are in good agreement with the results of the X-ray diffraction analyses. Even though the overall elemental composition could not be determined exclusively by EDX, a combination of XRD, HRTEM/SAED, EDX, and theoretical data allows for reliable assignment of the chemical compositions to the investigated samples.

2.6. Total energy calculations

Band structure calculations were carried out on $BaLi_4$ and the idealized $BaLi_2In_2$ structures at the DFT level using the full-potential LAPW method implemented in the WIEN2k package (version 06) [40] with the Perdew–Burke–Ernzerhof GGA exchange correlation potential. [41] The energy cutoff between the core and valence states was increased to −4 Ry in order to

treat the Ba 4*d* states as core levels, while 5*s* and 5*p* states comprised the semi-core levels. Scalar-relativistic calculations were run with 12 *k* points in the irreducible wedge of the Brillouin zone, corresponding to 95 *k* points in the whole BZ. The geometry was optimized by minimizing the total energy as a function of the unit cell volume and *c*/*a* ratio combined with the optimization of the internal structural parameters.

3. Results and discussion

The compound $BaLi_{2.1}In_{1.9}$ crystallizes in the hexagonal system, space group $P6_3/mmc$. Details of the data collection and structure refinement for this compound are listed in Table 1. Positional and anisotropic displacement parameters are given in Tables 2 and 3. It should be noted that in this system there are two different structures with the composition BaM_4 (M=Li or In), namely $BaIn_4$ ($BaAl_4$-type) and $BaLi_4$. The ternary phase $BaLi_{2.1}In_{1.9}$ belongs to the $BaLi_4$ structure type, however, the transition to the $BaAl_4$ type is not excluded in the phases with higher In content, which is the subject of future investigations. The structure of $BaLi_4$ was previously described in detail [42], so only a general comment and a comparison with the new compound will be provided. Three of four lithium positions in this structure are statistically occupied by Li and In atoms, however, always with ca. 90% of one element. Li together with In forms rows of centered face-sharing icosahedra along the *c* axis (Fig. 1). Positions in the center of the icosahedra are occupied only by Li atoms, while In atoms are situated mostly in the equatorial positions. Ba–Ba, Ba–Li, and Li–Li interatomic distances are in the ranges 4.2586(9)–4.509(1), 3.59(1)–3.81(2), and 2.76(2)–3.11(3) Å, respectively, hence somewhat shorter than in $BaLi_4$, showing the presence of the more electronegative element. Ba–In and Li–In distances (3.595(1)–3.87(1) and 2.87(1)–3.039(2) Å) are similar to those found in other Li–In compounds. Shortening of the interatomic distances due to the incorporation of In atoms is also reflected in the 15% smaller unit cell volume of $BaLi_{2.1}In_{1.9}$ (785 Å^3) in comparison to that of $BaLi_4$ (926.3 Å^3).

The crystal structure of $BaLi_{1.12}In_{0.98}$ is very similar to that of $Na_8K_{23}Cd_{12}In_{48}$ [43], however, some features are slightly

Table 2
Atomic coordinates, equivalent/isotropic thermal displacement parameters, and site occupancies for $BaLi_{2.1}In_{1.9}$.

Atom	Site	*x*	*y*	*z*	$U_{eq/iso}$	*G*
Ba1	6*h*	0.52227(8)	0.47773(8)	0.2500	0.0158(4)	1
In1	12*k*	0.16500(7)	0.3300(1)	0.0631(1)	0.0141(3)	0.91(1)
Li1	12*k*	0.16500(7)	0.3300(1)	0.0631(1)	0.0141(3)	0.09(1)
In2	6*h*	0.199(3)	0.100(1)	0.2500	0.042(8)	0.07(1)
Li2	6*h*	0.199(3)	0.100(1)	0.2500	0.042(8)	0.93(1)
In3	4*f*	0.3333	0.6667	0.045(4)	0.02(1)	0.02(1)
Li3	4*f*	0.3333	0.6667	0.045(4)	0.02(1)	0.98(1)
Li4	2*a*	0	0	0	0.04(2)	1

Table 3
Anisotropic displacement parameters for $BaLi_{2.1}In_{1.9}$.

	U_{11}	U_{22}	U_{33}	U_{23}	U_{13}	U_{12}
Ba1	0.0125(5)	U_{11}	0.0199(6)	0	0	0.0044(5)
In1	0.0130(4)	0.0124(5)	0.0165(5)	−0.0013(4)	−0.0007(2)	0.0062(3)
Li1	0.0130(4)	0.0124(5)	0.0165(5)	−0.0013(4)	−0.0007(2)	0.0062(3)

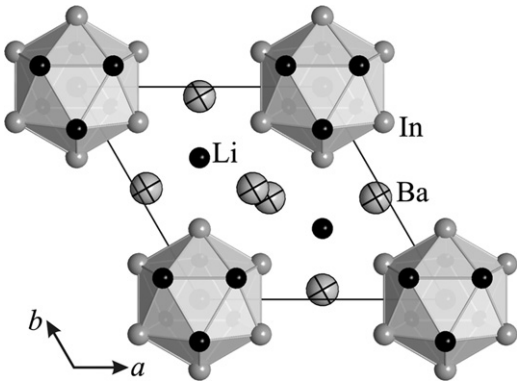

Fig. 1. Crystal structure of $BaLi_{2.1}In_{1.9}$ viewed along the *c* axis.

Table 1
Details of the crystal structure investigation and refinement for $BaLi_{2.1}In_{1.9}$, $BaLi_{1.12}In_{0.98}$, $BaLi_{1.02}In_{1.08}$, and $BaLi_{1.06}In_{1.16}$.

Empirical formula	$BaLi_{2.1}In_{1.9}$	$BaLi_{1.12}In_{0.98}$	$BaLi_{1.02}In_{1.08}$	$BaLi_{1.06}In_{1.16}$
Formula weight	370.61	258.87	270.04	277.75
Temperature, K		293(2)		
Wavelength, Å		0.56086		
Crystal system		hexagonal		trigonal
Space group	$P6_3/mmc$	$P6/mmm$		R-3c
a, Å	10.410(2)	17.469(1)	17.467(3)	18.894(3)
c, Å	8.364(2)	10.6409(7)	10.648(2)	85.289(17)
Volume, Å^3	785.0(2)	2812.3(8)	2813.5(8)	26368(8)
Z	6	30		276
Density (calculated), g cm^{-3}	4.704	4.584	4.781	4.828
μ, mm^{-1}	15.58	16.262	16.893	16.933
F(0 0 0)	934	3232	3279	32006
θ range	3.32–31.96°	3.7–39.4°	3.3–36.7°	1.3–23.5°
Index ranges	$-15 \le h, k \le 15$	$-25 \le h, k \le 25$	$-28 \le h, k \le 28$	$-21 \le h, k \le 21$
	$-12 \le l \le 12$	$-15 \le l \le 15$	$-17 \le l \le 17$	$-95 \le l \le 95$
Reflections collected	9133	41548	61828	52110
Independent reflections	554	1793	2712	4363
Refinement method		Full-matrix least-squares on F^2		
Data/restraints/parameters	554/0/19	1793/0/70	2712/0/66	4363/0/232
Data averaging	R_{int},=0.102, R_σ=0.036	R_{int},=0.141, R_σ=0.043	R_{int},=0.107, R_σ=0.026	R_{int},=0.192, R_σ=0.067
Goodness-of-fit on F^2	1.25	1.06	1.04	1.25
Final *R* indices [$I > 2\sigma(I)$][a]	*R*1=0.063, *wR*2=0.121	*R*1=0.032, *wR*2=0.072	*R*1=0.047, *wR*2=0.117	*R*1=0.061, *wR*2=0.116
R indices (all data)	*R*1=0.074, *wR*2=0.126	*R*1=0.054, *wR*2=0.077	*R*1=0.065, *wR*2=0.128	*R*1=0.169, *wR*2=0.151
Largest diff. peak and hole, e$^-$/Å^3	2.75 and −3.43	7.05 and −3.96	8.70 and −1.91	4.03 and −2.26

Table 4
Atomic coordinates, equivalent/isotropic thermal displacement parameters, and site occupancies for $BaLi_{1.12}In_{0.98}$.

Atom	Site	x	y	z	$U_{eq/iso}$	G
Ba1	4*h*	0.6667	0.3333	0.19727(9)	0.0210(2)	
Ba2	12*o*	0.78872(2)	0.57743(3)	0.29726(5)	0.0238(1)	
Ba3	6*k*	−0.38638(5)	0	0.5	0.0323(2)	
Ba4	6*l*	0.86463(3)	0.72925(6)	0	0.0281(2)	
Ba5	2*e*	0	0	−0.3130(3)	0.0408(8)	0.778(8)
Ba6	2*e*	0	0	0.146(1)	0.044(3)	0.220(8)
Ba7	1*b*	0	0	−0.5	0.050(5)	0.20(1)
In1	12*p*	0.49339(7)	0.16256(7)	0	0.0158(3)	0.500(3)
Li1	12*p*	0.49339(7)	0.16256(7)	0	0.0158(3)	0.500(3)
In2	6*m*	0.39515(4)	0.79029(8)	0.5	0.0187(4)	0.653(5)
Li2	6*m*	0.39515(4)	0.79029(8)	0.5	0.0187(4)	0.347(5)
In3	12*o*	0.54894(4)	0.09789(9)	0.7590(1)	0.0155(4)	0.381(3)
Li3	12*o*	0.54894(4)	0.09789(9)	0.7590(1)	0.0155(4)	0.619(3)
In4	12*n*	−0.64391(4)	0.0000	0.14610(7)	0.0154(2)	0.756(4)
Li4	12*n*	−0.64391(4)	0.0000	0.14610(7)	0.0154(2)	0.244(4)
In5	6*m*	0.10956(5)	0.2191(1)	0.5	0.0218(5)	0.544(5)
Li5	6*m*	0.10956(5)	0.2191(1)	0.5	0.0218(5)	0.456(5)
In6	12*n*	0	0.2021(2)	0.2888(3)	0.031(1)	0.222(4)
Li6	12*n*	0	0.2021(2)	0.2888(3)	0.031(1)	0.778(4)
Li7	3*f*	0.5	0	0	0.019(6)	

Table 5
Anisotropic displacement parameters for $BaLi_{1.12}In_{0.98}$.

Atom	U_{11}	U_{22}	U_{33}	U_{23}	U_{13}	U_{12}
Ba1	0.0202(2)	0.0202(2)	0.0224(5)	0	0	0.0101(1)
Ba2	0.0250(2)	0.0240(3)	0.0221(3)	−0.0018(2)	−0.0009(1)	0.0120(1)
Ba3	0.0378(3)	0.0375(5)	0.0213(4)	0	0	0.0187(2)
Ba4	0.0248(3)	0.0327(4)	0.0295(5)	0	0	0.0164(2)
Ba5	0.0274(7)	0.0274(7)	0.067(2)	0	0	0.0137(4)
Ba6	0.026(3)	0.026(3)	0.082(8)	0	0	0.013(1)
Ba7	0.038(5)	0.038(5)	0.074(12)	0	0	0.019(3)
In1	0.0165(5)	0.0148(5)	0.0163(6)	0	0	0.0079(4)
Li1	0.0165(5)	0.0148(5)	0.0163(6)	0	0	0.0079(4)
In2	0.0204(5)	0.0186(6)	0.0165(7)	0	0	0.0093(3)
Li2	0.0204(5)	0.0186(6)	0.0165(7)	0	0	0.0093(3)
In3	0.0164(5)	0.0148(6)	0.0149(7)	0.0015(5)	0.0008(2)	0.0074(3)
Li3	0.0164(5)	0.0148(6)	0.0149(7)	0.0015(5)	0.0008(2)	0.0074(3)
In4	0.0158(3)	0.0157(3)	0.0146(4)	0	0.0014(2)	0.0078(2)
Li4	0.0158(3)	0.0157(3)	0.0146(4)	0	0.0014(2)	0.0078(2)
In5	0.0228(6)	0.0228(8)	0.0199(9)	0	0	0.0114(4)
Li5	0.0228(6)	0.0228(8)	0.0199(9)	0	0	0.0114(4)
In6	0.026(1)	0.035(1)	0.028(2)	0.010(1)	0	0.0133(7)
Li6	0.026(1)	0.035(1)	0.028(2)	0.010(1)	0	0.0133(7)
Li7	0.018(9)	0.03(1)	0.01(1)	0	0	0.014(7)

Table 6
Atomic coordinates, equivalent/isotropic thermal displacement parameters, and site occupancies for $BaLi_{1.06}In_{1.16}$.

Atom	Site	x	y	z	$U_{eq/iso}$	G
Ba1	18*e*	0.6667	0.9795(2)	0.0833	0.0274(9)	
Ba2	36*f*	0.8005(2)	0.9966(2)	0.04644(3)	0.0249(6)	
Ba3	36*f*	0.5325(2)	0.8600(2)	0.04456(3)	0.0248(6)	
Ba4	36*f*	0.4694(2)	0.9968(2)	0.02105(3)	0.0292(6)	
Ba5	36*f*	0.8618(2)	0.1908(2)	0.02029(3)	0.0297(7)	
Ba6	36*f*	0.6706(2)	0.7844(2)	0.02281(3)	0.0304(7)	
Ba7	12*c*	0	0	0.06224(5)	0.023(1)	
Ba8	36*f*	0.5371(2)	0.2057(2)	0.04375(3)	0.0301(6)	
Ba9	18*e*	0.6667	0.1977(2)	0.0833	0.032(1)	
Ba10	12*c*	0.3333	0.6667	0.05889(6)	0.030(1)	
In1	36*f*	0.6679(2)	0.8028(2)	0.06507(3)	0.018(1)	0.98(1)
Li1	36*f*	0.6679(2)	0.8028(2)	0.06507(3)	0.018(1)	0.02(1)
In2	36*f*	0.6657(2)	0.0936(2)	0.04472(4)	0.026(1)	0.94(1)
Li2	36*f*	0.6657(2)	0.0936(2)	0.04472(4)	0.026(1)	0.06(1)
In3	18*e*	0.4496(2)	0.1163(2)	0.0833	0.018(2)	0.96(2)
Li3	18*e*	0.4496(2)	0.1163(2)	0.0833	0.018(2)	0.04(2)
In4	36*f*	0.3526(2)	0.0216(2)	0.05357(4)	0.019(1)	0.89(1)
Li4	36*f*	0.3526(2)	0.0216(2)	0.05357(4)	0.019(1)	0.11(1)
In5	36*f*	0.8938(2)	0.0806(2)	0.08437(3)	0.017(1)	0.95(1)
Li5	36*f*	0.8938(2)	0.0806(2)	0.08437(3)	0.017(1)	0.05(1)
In6	36*f*	0.4952(2)	0.8250(2)	0.00211(4)	0.029(1)	0.85(1)
Li6	36*f*	0.4952(2)	0.8250(2)	0.00211(4)	0.029(1)	0.15(1)
In7	36*f*	0.9969(2)	0.0962(2)	0.02614(4)	0.021(2)	0.72(1)
Li7	36*f*	0.9969(2)	0.0962(2)	0.02614(4)	0.021(2)	0.28(1)
In8	36*f*	0.6669(3)	0.9926(3)	0.01289(6)	0.025(2)	0.57(1)
Li8	36*f*	0.6669(3)	0.9926(3)	0.01289(6)	0.025(2)	0.43(1)
In9	36*f*	0.5137(2)	0.6553(3)	0.05299(6)	0.019(2)	0.57(1)
Li9	36*f*	0.5137(2)	0.6553(3)	0.05299(6)	0.019(2)	0.43(1)
In10	36*f*	0.8395(3)	0.9939(3)	0.00593(7)	0.025(2)	0.52(1)
Li10	36*f*	0.8395(3)	0.9939(3)	0.00593(7)	0.025(2)	0.48(1)
In11	36*f*	0.4315(4)	0.6648(4)	0.02167(7)	0.026(3)	0.44(1)
Li11	36*f*	0.4315(4)	0.6648(4)	0.02167(7)	0.026(3)	0.56(1)
In12	36*f*	0.9883(5)	0.1791(5)	0.0544(1)	0.015(4)	0.26(1)
Li12	36*f*	0.9883(5)	0.1791(5)	0.0544(1)	0.015(4)	0.74(1)
In13	36*f*	0.8288(6)	0.1766(6)	0.1020(1)	0.026(4)	0.25(1)
Li13	36*f*	0.8288(6)	0.1766(6)	0.1020(1)	0.026(4)	0.75(1)
In14	12*c*	0.3333	0.6667	-0.0102(5)	0.075(17)	0.21(3)
Li14	12*c*	0.3333	0.6667	-0.0102(5)	0.075(17)	0.79(3)
In15	36*f*	0.3459(7)	0.1709(7)	0.0652(1)	0.010(5)	0.18(1)
Li15	36*f*	0.3459(7)	0.1709(7)	0.0652(1)	0.010(5)	0.82(1)
In16	36*f*	0.5023(9)	0.6666(8)	-0.0107(2)	0.026(6)	0.16(1)
Li16	36*f*	0.5023(9)	0.6666(8)	-0.0107(2)	0.026(6)	0.84(1)
In17	36*f*	0.816(2)	0.899(2)	0.0847(3)	0.03(1)	0.08(1)
Li17	36*f*	0.816(2)	0.899(2)	0.0847(3)	0.03(1)	0.92(1)
Li18	36*f*	0.749(3)	0.724(3)	0.0853(6)	0.01(1)	
Li19	6*b*	0	0	0	0.09(9)	

different. The new ternary phase crystallizes with hexagonal symmetry. Details of the data collection and structure refinement, positional and displacements parameters for this compound are listed in Tables 1–7. The main structural features are In/Li icosahedra and tunnels along the *c* axis with Ba atoms inside (Fig. 2). For a comparison, the complicated structure of $Na_8K_{23}Cd_{12}In_{48}$ can be written as $Na_6K_{22}(Na_2K)Cd_{12}(In_{12}\square)_3In_6(In_3)_2$ with the following structural units: empty $In_{12}\square$ icosahedra, In_3 triangles, and hexagonal tubes around 00*z* with the composition $Cd_{12}In_6Na_6$. Each tube is filled with linear chains of composition Na_2K. In addition, 22 potassium atoms are distributed between these main structural units. In analogy to the description above, thirty formula units $BaLi_{1.12}In_{0.98}$ can be approximately described as $Ba_6Ba_{22}(Ba_{2.2})(M_{12})(M_{12}Li)_3M_6(M_3)_2$ where *M* stands for a statistical mixture of In and Li. The crystal structure of $BaLi_{1.12}In_{0.98}$ differs from that of $Na_8K_{23}Cd_{12}In_{48}$ mainly in the following: the M_{12} icosahedra are centered by Li atoms (compared to the empty $In_{12}\square$ icosahedra) and different positions in the tube are occupied by disordered Ba atoms in three positions with occupation factors ranging from 0.2 to 0.78 adding up to a total of 2.2 (compared to the ordered Na_2K tube filling).

All Li and Li/In atoms are coordinated by icosahedra, those of the atoms forming the tube being considerably distorted. Ba atoms form the Frank–Kasper polyhedra with the coordination numbers 15 and 16. Ba–Ba, Ba–In, and In–In interatomic distances are in the ranges 3.8431(5)–4.3176(9), 3.315(2)–3.926(3), and 2.869(3)–3.315(2) Å, respectively, similar to those found in binary Ba–In compounds.

A measurement on a second crystal from the same batch resulted in practically the same structure, however, with only two partially occupied Ba sites in the tube adding up to 2.3 Ba atoms in slightly different positions and a slightly different overall composition $BaLi_{1.02}In_{1.08}$. Additional weak peaks along 00*z* could be refined as 4–5% occupied Ba positions with distances of 0.5–0.8 Å to the nearest Ba atom with no changes to the general composition (Fig. 3). Similar smeared out electron density along the *c* axis was also found in the compounds $K_{1.76}Au_6In_4$ and $K_{0.73}Au_2In_2$ [44], for example, where the *K* atoms are situated in the tunnels formed from the more electronegative elements.

Table 7
Anisotropic displacement parameters for $BaLi_{1.06}In_{1.16}$.

Atom	U_{11}	U_{22}	U_{33}	U_{23}	U_{13}	U_{12}
Ba1	0.021(2)	0.021(1)	0.040(2)	0.0013(9)	0.003(2)	0.0105(9)
Ba2	0.019(1)	0.019(1)	0.032(2)	0.002(1)	0.001(1)	0.006(1)
Ba3	0.019(1)	0.028(1)	0.030(2)	0.000(1)	−0.000(1)	0.013(1)
Ba4	0.030(1)	0.028(1)	0.030(1)	0.002(1)	0.005(1)	0.014(1)
Ba5	0.031(2)	0.028(1)	0.033(2)	−0.004(1)	−0.002(1)	0.017(1)
Ba6	0.030(2)	0.032(2)	0.028(2)	0.0001(1)	0.003(1)	0.014(1)
Ba7	0.022(1)	0.022(1)	0.026(2)	0	0	0.0111(7)
Ba8	0.026(1)	0.023(1)	0.039(2)	0.001(1)	0.001(1)	0.010(1)
Ba9	0.014(2)	0.029(2)	0.049(2)	0.0003(9)	0.001(2)	0.0070(9)
Ba10	0.024(2)	0.024(2)	0.042(3)	0	0	0.0117(7)
In1	0.016(2)	0.016(2)	0.021(2)	0.002(1)	0.000(1)	0.008(1)
In2	0.025(2)	0.024(2)	0.030(2)	0.002(2)	0.002(1)	0.012(2)
In3	0.014(2)	0.014(2)	0.024(3)	0.0007(9)	−0.0007(9)	0.005(2)
In4	0.016(2)	0.018(2)	0.023(2)	−0.000(1)	0.002(1)	0.009(1)
In5	0.015(2)	0.011(2)	0.025(2)	−0.001(1)	0.001(1)	0.005(1)
In6	0.028(2)	0.025(2)	0.038(3)	0.004(2)	0.008(2)	0.017(2)
In7	0.020(2)	0.017(2)	0.023(2)	−0.001(2)	−0.001(2)	0.008(2)
In8	0.018(3)	0.029(3)	0.025(3)	0.001(2)	0.000(2)	0.008(2)
In9	0.011(3)	0.017(3)	0.026(3)	−0.002(2)	−0.001(2)	0.006(2)
In10	0.024(3)	0.024(3)	0.032(4)	−0.005(3)	0.001(3)	0.014(3)
In11	0.017(4)	0.026(4)	0.027(4)	0.001(3)	−0.002(3)	0.005(3)
In12	0.012(5)	0.010(5)	0.018(6)	−0.002(4)	0.003(4)	0.002(4)
In13	0.027(7)	0.023(6)	0.032(8)	0.007(5)	0.001(5)	0.015(5)
In14	0.036(14)	0.036(14)	0.15(4)	0.000	0.000	0.018(7)
In15	0.008(7)	0.017(7)	0.012(7)	0.002(5)	0.006(5)	0.010(5)
In16	0.028(9)	0.012(8)	0.033(10)	0.000(6)	0.011(7)	0.007(7)
Li1	0.016(2)	0.016(2)	0.021(2)	0.002(1)	0.0000(13)	0.008(1)
Li2	0.025(2)	0.024(2)	0.030(2)	0.002(2)	0.002(1)	0.012(2)
Li3	0.014(2)	0.014(2)	0.024(3)	0.0007(9)	−0.0007(9)	0.005(2)
Li4	0.016(2)	0.018(2)	0.023(2)	−0.000(1)	0.002(1)	0.009(1)
Li5	0.015(2)	0.011(2)	0.025(2)	−0.001(1)	0.001(1)	0.005(1)
Li6	0.028(2)	0.025(2)	0.038(3)	0.004(2)	0.008(2)	0.017(2)
Li7	0.020(2)	0.017(2)	0.023(2)	−0.001(2)	−0.001(2)	0.008(2)
Li8	0.018(3)	0.029(3)	0.025(3)	0.001(2)	0.000(2)	0.008(2)
Li9	0.011(3)	0.017(3)	0.026(3)	−0.002(2)	−0.001(2)	0.006(2)
Li10	0.024(3)	0.024(3)	0.032(4)	−0.005(3)	0.001(3)	0.014(3)
Li11	0.017(4)	0.026(4)	0.027(4)	0.001(3)	−0.002(3)	0.005(3)
Li12	0.012(5)	0.010(5)	0.018(6)	−0.002(4)	0.003(4)	0.002(4)
Li13	0.027(7)	0.023(6)	0.032(8)	0.007(5)	0.001(5)	0.015(5)
Li14	0.036(14)	0.036(14)	0.15(4)	0.000	0.000	0.018(7)
Li15	0.008(7)	0.017(7)	0.012(7)	0.002(5)	0.006(5)	0.010(5)
Li16	0.028(9)	0.012(8)	0.033(10)	0.000(6)	0.011(7)	0.007(7)

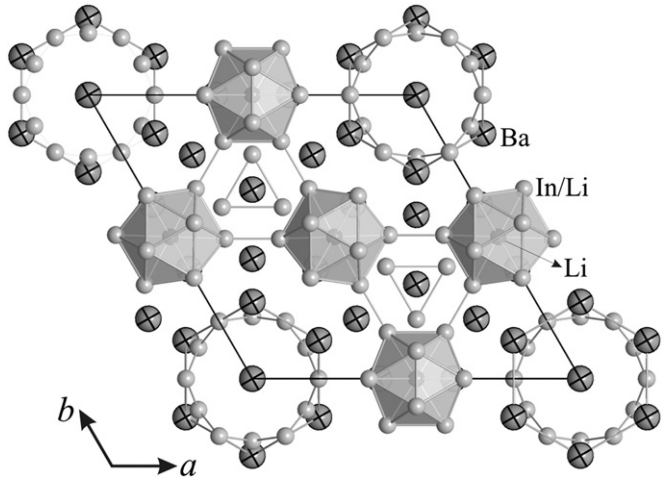

Fig. 2. Crystal structure of $BaLi_{1.12}In_{0.98}$ viewed along the *c* axis.

$BaLi_{1.06}In_{1.16}$≡$Ba_{23}(Li,In)_{51}$ crystallizes in the rhombohedral system, space group *R*-3*c*. Details of the data collection and structure refinement for this compound are listed in Table 1. Positional and anisotropic displacement parameters are given in Tables 8 and 9. The compound has the structure of $Li_{33.3}Ba_{13.1}Ca_3$≡$(Ba,Ca)_{23}(Li,Ca)_{51}$ [7]. Similar to both previous phases, two different polytetrahedral clusters were found: centered icosahedra M_{13} and clusters of two interpenetrating icosahedra, M_{19} (*M*=Li/In). The latter was also observed in $Ba_{19}Li_{44}$-type compounds [45,46]. In the structure of $BaLi_{1.06}In_{1.16}$ all Ba positions are fully occupied and all In and Li positions are statistically occupied with different ratios of the metals except for the pure Li central positions in the M_{13} icosahedra and M_{19} double icosahedra. The Ba atom substructure contains only two polyhedron types, face-sharing double octahedra and interpenetrating double tetrahedra, both together forming cages which surround the Li/In clusters. An appropriate section of the structure is shown as the projection along the *c* axis in Fig. 4. Ba–Ba, Ba–Li/In, and In/Li–In/Li interatomic distances lie in the ranges 3.755(5)–4.470(1), 3.52(1)–4.16(1), and 2.83(5)–3.35(2) Å, respectively, comparable to those found in $BaLi_{1.12}In_{0.98}$.

$Li_{35}In_{45}Ba_{39}N_9$ crystallizes in the tetragonal system, space group *I*-42*m*. Crystallographic information and details of the data collection are presented in Tables 8–10. The new ternary phase is isostructural with the previously reported subnitride $Li_{80}Ba_{39}N_9$ [2]. Similar to the latter, the crystal structure of $Li_{35}In_{45}Ba_{39}N_9$ can be described as a packing of five different fragments, $(Li,In)_{17}$ polytetrahedral clusters, In_3 triangles, forming bridges between these clusters, Ba_4 tetrahedra, Ba_6N and $Ba_5N_6(Li,In)_{12}$ nitride clusters. While the Ba and N positions are fully occupied by the respective atoms, most In/Li positions are statistically occupied to a varying degree. In contrast to the compounds discussed earlier, the positions inside the icosahedra are occupied by both Li as the majority (ca. 80%) and In atoms. A second finding to be mentioned is the fact that the cluster $Ba_5N_6Li_{12}$ in $Li_{80}Ba_{39}N_9$ is now partly substituted in the Li positions by In. Thus, indium joins the two other metals in bonding to nitrogen. In comparison to $Li_{80}Ba_{39}N_9$, the quaternary phase has smaller cell parameters and shorter Ba–Ba (4.307(4)–4.574(7) Å) and Ba–Li/In (3.53(5)–4.04(5) Å) interatomic distances in the metallic part of the structure, similar to the three previous In-containing phases. Because of the proximity of the nitrogen atoms to the indium atoms, the nitrogen atom positions could not be refined accurately. In/Li–N contacts are very short (1.59(1)–1.60(2) Å), but similar to those found in $Li_{80}Ba_{39}N_9$ (d_{Li-N}=1.73–1.75 Å), perhaps due to the small number of nearest nitrogen neighbors, namely only two Li/In atoms and one Ba atom. It should be noted that in contrast to gallium-containing compounds no subnitride with bonding between fully occupied indium and nitrogen sites has been found.

$LiIn_2Ba_3N_{0.83}$, the second identified representative of the Li–In–Ba–N system, crystallizes in the cubic crystal system, space group *Fd*-3*m*. Details of the data collection and structure refinement, positional and displacements parameters for this compound are listed in Tables 8, 11, and 12. Its crystal structure can be described as a 3D network of corner-sharing Ba_6N octahedra (Fig. 5) with Li_4In_4 tetrahedral star-like clusters filling the voids. Each Ba_6N unit has common corners with six others forming empty octahedra between each four of them. The Li_4In_4 cluster consists of a central In_4 tetrahedron with every face capped by a Li atom without mixed occupation at these positions.

Such In_4 tetrahedra were observed in the binary compound Na_2In [47]. Each of the capping Li atoms is common to two Li_4In_4 clusters forming bridges between them, which results in another 3D substructure. The coordination polyhedron for both Li and In is an icosahedron, however, strongly distorted for In in the center. The crystal structure of $LiIn_2Ba_3N_{0.83}$ is similar to that of $Li_{0.92}In_{4.32}Sr_6N_{2.49}$ [15] (upon doubling the formula unit), but the two compounds cannot be called isostructural as the second N position is now empty in the new subnitride. The Li position is in

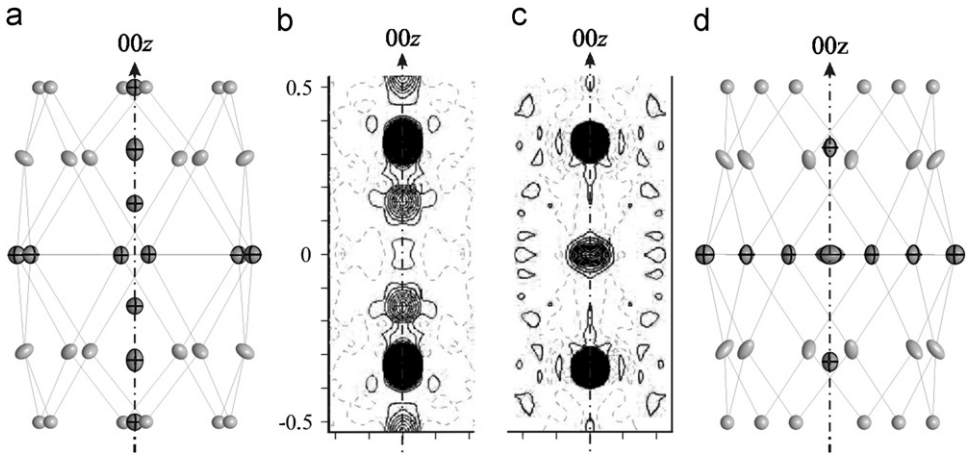

Fig. 3. Atom arrangement and Fourier maps around the origin of the unit cell along the *c* axis in the structures of $BaLi_{1.12}In_{0.98}$ (a, b) and $BaLi_{1.02}In_{1.08}$ (d, c).

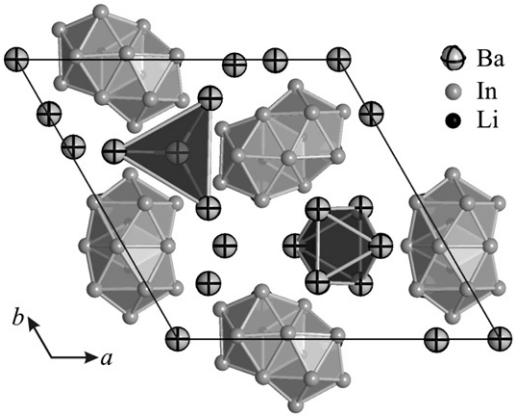

Fig. 4. Crystal structure of $BaLi_{1.06}In_{1.16}$ viewed along the *c* axis.

Table 8
Details of the crystal structure investigation and refinement for $Li_{35}In_{45}Ba_{39}N_9$ and $LiIn_2Ba_3N_{0.83}$.

Empirical formula	$Li_{35}In_{45}Ba_{39}N_9$	$LiIn_2Ba_3N_{0.83}$
Formula weight	10905.57	1320.60
Temperature, K	293(2)	
Wavelength, Å	0.56086	
Crystal system	tetragonal	cubic
Space group	*I*-42*m*	*Fd*-3*m*
a, Å	15.299(2)	14.913(2)
c, Å	30.682(6)	–
Volume, Å^3	7182(2)	3316.7(7)
Z	2	8
Density (calculated), g · cm^{-3}	5.045	5.289
μ, mm^{-1}	17.568	19.406
F(000)	9128	4398
θ range	2.3° to 17.5°	3.86° to 36.67
Index ranges	$-12 \le h, k \le 12$, $-25 \le l \le 25$	$-24 \le h, k, l \le 24$
Reflections collected	9831	15850
Independent reflections	1227	437
Refinement method	Full-matrix least-squares on F^2	
Data/restraints/parameters	1227/0/135	437/0/13
Data averaging	$R_{int,}$=0.176, R_σ=0.086	$R_{int,}$=0.070, R_σ=0.014
Goodness-of-fit on F^2	0.92	1.24
Final *R* indices [$I > 2\sigma(I)$][a]	*R*1=0.052, *wR*2=0.116	*R*1=0.034, *wR*2=0.079
R indices (all data)	*R*1=0.074, *wR*2=0.123	*R*1=0.034, *wR*2=0.078
Largest diff. peak and hole, e$^-$/Å^3	4.18 and −1.48	1.29 and −2.70

contrast to the phase with Sr fully occupied, and no In was found there. The In–In separations (3.0399(2) Å) are somewhat shorter than Li–In contacts (3.1438(3) Å), however, compare well with those found in binary Ba–In compounds. In addition, both quaternary subnitrides $LiIn_2Ba_3N_{0.83}$ and $Li_{0.92}In_{4.32}Sr_6N_{2.49}$ feature the metal atom arrangement similar to that in NaBa [48], with lithium and indium atoms occupying the Na sites, while the alkaline-earth metal subnetworks in all three structures are identical. Full occupation of the nitrogen position in $LiIn_2Ba_3N_{0.83}$ on the other hand would result in an isostructural relationship to Fe_3W_3C [49], with Ba and N atoms taking the W and C positions, respectively, and Li and In atoms ordered on the Fe sites. See also Ref. [15] for a detailed discussion of these structure types.

The electron microscopy investigations were performed on a heterogeneous sample containing $BaLi_{1.12}In_{0.98}$ and $BaLi_{1.06}In_{1.16}$. The crystal structures of both phases could be verified by electron diffraction. The precession electron diffraction (PED) patterns of Figs. 6 and 7 were recorded on $BaLi_{1.12}In_{0.98}$ and $BaLi_{1.06}In_{1.16}$, respectively. This finding is supported by the observed ratios Ba:In=1.05(3) and Ba:In=0.80(4), respectively. Assuming the kinematic approximation, the patterns of $BaLi_{1.12}In_{0.98}$ (Fig. 6) convincingly match the simulated patterns based on the average structures derived by XRD. Even the PED patterns of Fig. 7 ($BaLi_{1.06}In_{1.16}$) exhibit such good correlation, however, including higher order Laue zones, cf. crowded superposition at high resolution (Fig. 7, zone axis [2 1 0]). For both compounds the disorder on the mixed and randomly occupied atom positions is evident by the absence of any characteristic scattering phenomenon, e.g. structured diffuse scattering or superstructure intensity. Additionally, the Fourier transforms of high resolution images show no signs of ordering inside discrete domains.

Generally, the agreement of experimental and simulated HRTEM micrographs based on the average structure appears satisfactory, e.g. Fig. 8b and c ($BaLi_{1.12}In_{0.98,}$ zone axis [1 0 1]) and ($BaLi_{1.06}In_{1.16}$, zone axis [2 1 0]), respectively. This includes minute differences between the related structures. For instance, the bright double spots in simulated micrographs of Fig. 8a can be connected by a straight line for $BaLi_{1.12}In_{0.98}$ (left), but not for $BaLi_{1.06}In_{1.16}$ (right). This detail becomes even more apparent when turning the page and looking along the line at glancing angle. Moreover, only for $BaLi_{1.12}In_{0.98}$ (Fig. 8a, right) the double spots appear with alternating brighter and darker contrast as they correlate with the superposition of Ba and Ba with mixed Li/In

Table 9
Atomic coordinates, equivalent/isotropic thermal displacement parameters, and site occupancies for $Li_{35}In_{45}Ba_{39}N_9$.

Atom	Site	x	y	z	$U_{eq/iso}$	G
Ba1	4e	0	0	0.0888(2)	0.022(2)	
Ba2	8h	0.5	0	0.1604(1)	0.020(2)	
Ba3	16j	0.0027(3)	0.3205(2)	0.25243(11)	0.020(1)	
Ba4	16j	0.4071(2)	0.1054(2)	0.04653(9)	0.016(1)	
Ba5	8i	0.1057(3)	0.1057(3)	0.1952(2)	0.026(2)	
Ba6	8i	0.4048(2)	0.4048(2)	0.1968(2)	0.022(2)	
Ba7	8f	0	0.1807(3)	0	0.019(1)	
Ba8	2b	0.5	0.5	0	0.028(3)	
Ba9	8i	0.3494(3)	0.3494(3)	0.0748(2)	0.031(2)	
In1	8i	0.1799(3)	0.1799(3)	0.0860(2)	0.016(2)	
In2	16j	0.3268(3)	0.1803(3)	0.1601(1)	0.020(1)	
In3	16j	0.3581(2)	−0.1241(3)	0.0709(1)	0.022(1)	
In4	8i	0.1415(3)	0.1415(3)	0.3115(2)	0.025(2)	
In5	8i	−0.1282(3)	0.1282(3)	0.1864(2)	0.030(2)	
In6	16j	0.251(3)	−0.007(4)	0.125(2)	0.01(3)	0.03(2)
Li6	16j	0.251(3)	−0.007(4)	0.125(2)	0.01(3)	0.97(2)
In7	8i	−0.1679(5)	0.1679(5)	0.0944(4)	0.034(7)	0.52(3)
Li7	8i	−0.1679(5)	0.1679(5)	0.0944(4)	0.034(7)	0.48(3)
In8	16j	−0.3136(6)	0.1683(5)	0.1659(2)	0.032(4)	0.57(2)
Li8	16j	−0.3136(6)	0.1683(5)	0.1659(2)	0.032(4)	0.43(2)
In9	8i	−0.247(5)	0.247(5)	0.245(3)	0.01(5)	0.01(2)
Li9	8i	−0.247(5)	0.247(5)	0.245(3)	0.01(5)	0.99(2)
In10	16j	0.2557(7)	0.0260(7)	0.3722(3)	0.005(7)	0.27(2)
Li10	16j	0.2557(7)	0.0260(7)	0.3722(3)	0.005(7)	0.73(2)
In11	8i	−0.2434(8)	0.2434(8)	0.0138(5)	0.02(1)	0.29(2)
Li11	8i	−0.2434(8)	0.2434(8)	0.0138(5)	0.02(1)	0.71(2)
In12	16j	0.4298(4)	−0.2872(4)	0.0353(2)	0.011(3)	0.54(2)
Li12	16j	0.4298(4)	−0.2872(4)	0.0353(2)	0.011(3)	0.46(2)
In13	8i	0.0701(5)	0.0701(5)	0.3931(3)	0.018(6)	0.51(3)
Li13	8i	0.0701(5)	0.0701(5)	0.3931(3)	0.018(6)	0.49(3)
In14	8i	0.817(3)	0.183(3)	0.594(2)	0.12(4)	0.14(4)
Li14	8i	0.817(3)	0.183(3)	0.594(2)	0.12(4)	0.86(4)
N1	4d	0.5	0	0.25	0.03(2)	
N2	2e	0	0	0	0.03(2)	
N3	4e	0	0	0.410(2)	0.05(5)	
N4	8g	0.5	−0.317(3)	0	0.05(5)	

Table 10
Anisotropic displacement parameters for $Li_{35}In_{45}Ba_{39}N_9$.

Atom	U_{11}	U_{22}	U_{33}	U_{23}	U_{13}	U_{12}
Ba1	0.026(3)	0.026(3)	0.015(4)	0	0	0.006(4)
Ba2	0.030(3)	0.018(3)	0.011(3)	0	0	0.000(3)
Ba3	0.028(2)	0.017(2)	0.014(2)	0.001(2)	−0.002(2)	0.001(2)
Ba4	0.020(2)	0.020(2)	0.009(2)	−0.002(2)	−0.003(2)	−0.003(2)
Ba5	0.032(2)	0.032(2)	0.015(3)	−0.003(2)	−0.003(2)	0.004(3)
Ba6	0.025(2)	0.025(2)	0.016(3)	0.003(2)	0.003(2)	0.005(3)
Ba7	0.022(3)	0.015(3)	0.020(3)	0	0.005(2)	0
Ba8	0.032(4)	0.032(4)	0.018(6)	0	0	0
Ba9	0.032(2)	0.032(2)	0.028(3)	−0.010(2)	−0.010(2)	0.012(3)
In1	0.018(2)	0.018(2)	0.012(3)	0.006(2)	0.006(2)	0.008(3)
In2	0.024(3)	0.022(3)	0.014(2)	−0.005(2)	0.003(2)	−0.003(2)
In3	0.026(3)	0.026(3)	0.013(2)	0.004(2)	0.0025(18)	−0.001(2)
In4	0.031(3)	0.031(3)	0.012(3)	−0.006(2)	−0.006(2)	0.000(3)
In5	0.037(3)	0.037(3)	0.017(3)	0.001(2)	−0.001(2)	0.003(4)

Table 11
Atomic coordinates, equivalent/isotropic thermal displacement parameters, and site occupancies for $LiIn_2Ba_3N_{0.83}$.

Atom	Site	x	y	z	$U_{eq/iso}$	G
Ba1	48f	0.125	0.125	0.93610(3)	0.0172(1)	
In1	32e	0.05293(2)	0.05293(2)	0.69707(2)	0.0145(1)	
Li1	16d	0	0	0.5	0.013(4)	
N1	16c	0	0	1	0.019(3)	0.83(6)

Table 12
Anisotropic displacement parameters for $LiIn_2Ba_3N_{0.83}$.

Atom	U_{11}	U_{22}	U_{33}	U_{23}	U_{13}	U_{12}
Ba1	0.0195(2)	0.0195(2)	0.0125(2)	0	0	0.0040(1)
In1	0.0145(1)	0.0145(1)	0.0145(1)	0.00273(9)	0.00273(9)	−0.00273(9)
N1	0.019(3)	0.019(3)	0.019(3)	−0.002(2)	−0.002(2)	−0.002(2)
Li1	0.013(4)	0.013(4)	0.013(4)	0.008(4)	0.008(4)	0.008(4)

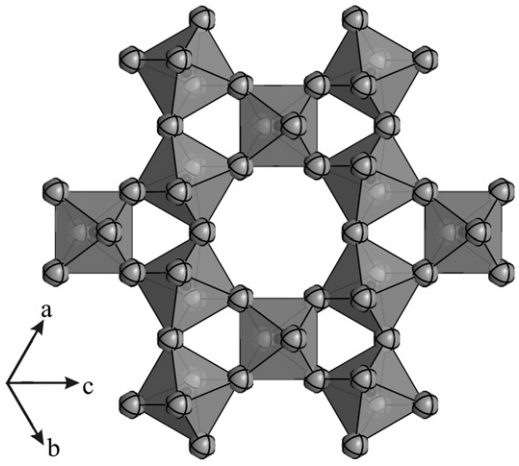

Fig. 5. Part of the barium substructure in $LiIn_2Ba_3N_{0.83}$ containing corner-sharing Ba_6N octahedra.

positions, respectively. For $BaLi_{1.06}In_{1.16}$ (Fig. 8a, left) all atoms correlating with the double spots are equivalent by average symmetry and thus appear with the same intensity. These minute details are well seen in the experimental images, however, on closer inspection unsystematic variations of the contrasts intensity can be identified. These deviations preferably occur on those positions which were refined as mixed Li/In positions for the average structures and thus can be rationalized in terms of deviations of the local Li/In distribution from the average values.

3.1. Theoretical calculations

In order to address the crystal volume reduction upon the substitution of lithium by indium in the reported intermetallic and subnitride phases, test calculation were carried out on $BaLi_4$ and the idealized structure of $BaLi_{2.1}In_{1.9}$, in which lithium atoms fully occupy the 2*a*, 4*f*, and 6*h* positions, while the 12*k* site is fully occupied by indium atoms, thus representing an ordered stoichiometric $BaLi_2In_2$ model which approximates the experimentally characterized $BaLi_{2.1}In_{1.9}$. Full structural optimization of the two intermetallic phases yielded somewhat smaller unit cells compared to the experimentally determined ones (Table 13). However, the trend towards smaller crystal volume in the In-substituted phase is clearly reproduced. This reduction is somewhat smaller compared to the experimental finding, which might be due to the lower assumed Li/In ratio or the absence of disorder in the model structure. The experimentally observed positional parameters in the crystal structures of $BaLi_4$ and $BaLi_{2.1}In_{1.9}$ remained unchanged in the course of total energy optimization due to nearly vanishing forces, manifesting a good agreement between theory and experiment.

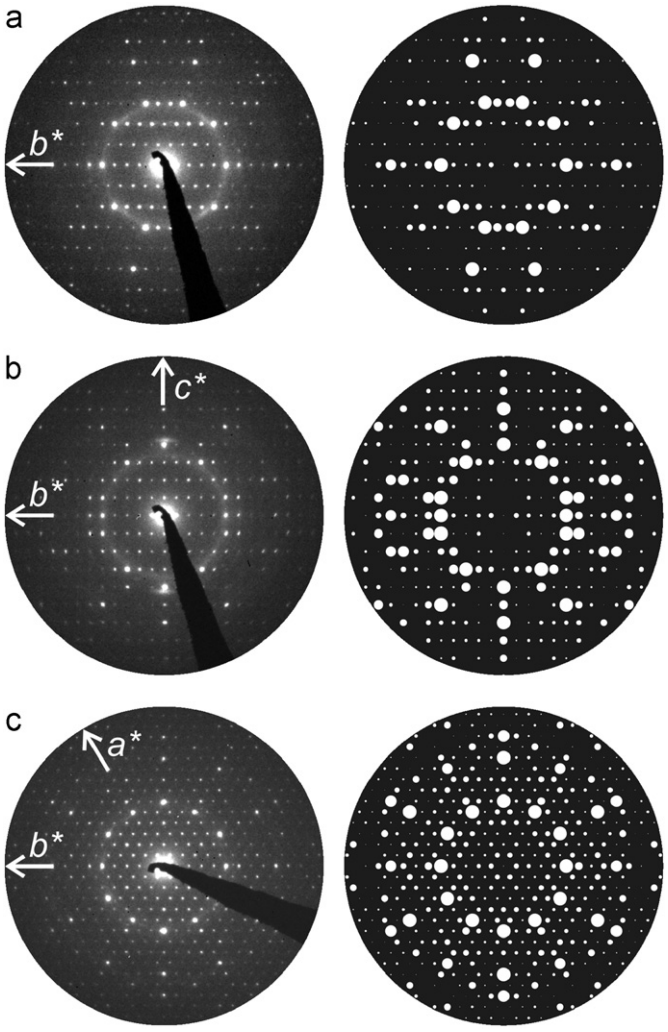

Fig. 6. Measured PED patterns for $BaLi_{1.12}In_{0.98}$ (left) with simulations based on the kinematic approximation (right): zone axes [1 0 1] (a), [1 0 0] (b), and [0 0 1] (c).

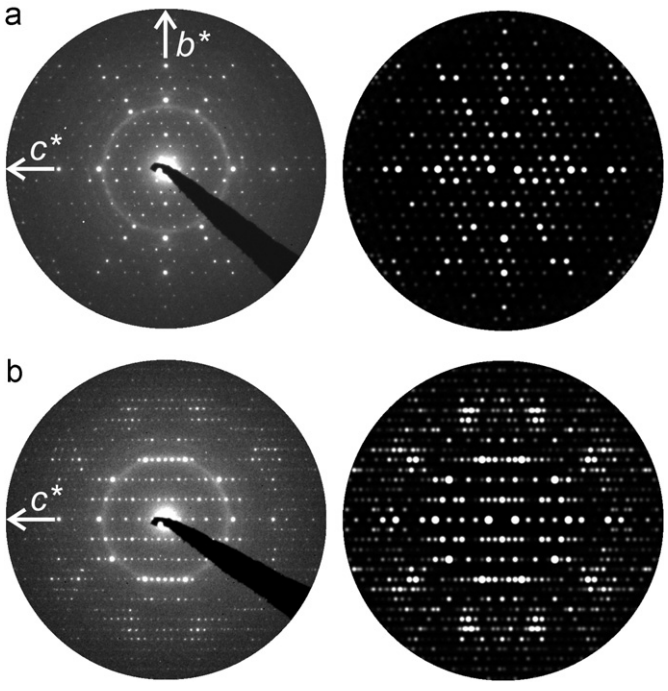

Fig. 7. Measured PED patterns for $BaLi_{1.06}In_{1.16}$ (left) with PED simulations (right, precession angle: 3°, thickness: 10 nm), zone axes [1 0 0] (a) and [2 1 0] (b).

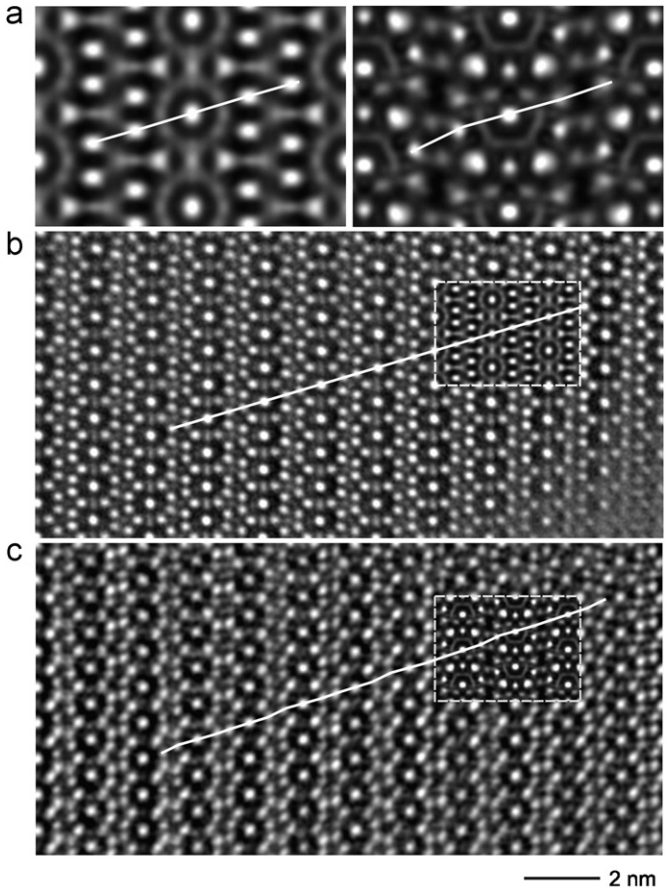

Fig. 8. (a) Simulated micrographs for $BaLi_{1.12}In_{0.98}$, zone axis [1 0 1] (left, thickness 8.2 nm, Δf= 80 nm) and $BaLi_{1.06}In_{1.16}$, zone axis [2 1 0] (right, thickness 9.8 nm, Δf= 75 nm); (b) and (c) experimental micrographs with inserted simulations for $BaLi_{1.12}In_{0.98}$, zone axis [1 0 1], and $BaLi_{1.06}In_{1.16}$, zone axis [2 1 0], respectively. Parameters for simulation were chosen as for (a). The solid white line is an eye guide connecting bright spots, see text for details.

Table 13
Experimental and theoretically optimized parameters (P) for $BaLi_4$ and $BaLi_{2.1}In_{1.9}$.

P	$BaLi_4$ [41]	$BaLi_2In_2$	Δ, %
Experimental[a]			
a, Å	10.936(1)	10.410(2)	−4.8
c, Å	8.943(2)	8.364(2)	−6.5
V/Z, Å^3	154.38	130.83	−15.3
Theoretical[b]			
a, Å	10.717	10.479	−2.2
c, Å	8.939	8.420	−5.8
V/Z, Å^3	148.20	133.44	−10.0

[a] for the experimentally observed composition $BaLi_{2.1}In_{1.9}$ with partial Li/In disorder.

[b] for the idealized stoichiometric $BaLi_2In_2$ model with indium atoms only in the 12k positions. $\left(\Delta = \frac{P_{BaLi_4} - P_{BaLi_2In_2}}{P_{BaLi_4}} \times 100\%\right)$

4. Summary

Two new subnitrides in the system Li–In–Ba–N and three Li–In–Ba intermetallic phases have been synthesized. In $BaLi_{2.1}In_{1.9}$ the In atoms were found to participate in compound formation within the parent $BaLi_4$ structure, however, $BaLi_{1.12}In_{0.98}$ does not have a binary analogue. Some Ba atoms in the structure of $BaLi_{1.12}In_{0.98}$ were found to be disordered along

the *c* axis similar to the potassium atom disorder in $K_{1.76}Au_6In_4$ and $K_{0.73}Au_2In_2$. $BaLi_{1.06}In_{1.16}$ is the third representative of the $Li_{33.3}Ba_{13.1}Ca_3$ structure type, which was not found in the binary Ba–Li system and is always stabilized by a third element. Considerable Li/In mixed occupancies are present in all three intermetallic phases as well as in $Li_{35}In_{45}Ba_{39}N_9$. Extended homogeneity ranges are expected for all these phases. $LiIn_{2-}Ba_3N_{0.83}$ was found to be different from the two related subnitrides $Ae_6In_4(In_xLi_y)N_{3-z}$ (Ae=Sr or Ba), featuring a lower nitrogen content and no mixed Li/In occupancies.

Acknowledgments

The authors thank Dr. C. Hoch for collecting the single-crystal diffraction data and for help in the structure determinations as well as Dr. V. Babizhetskyy for helpful discussions.

References

[1] A. Simon, in: M. Driess, N. Nöth (Eds.), Molecular Clusters of the Main Group Elements, Wiley-VCH, Weinheim, 2004, pp. 246–266.
[2] V. Smetana, V. Babizhetskyy, G.V. Vajenine, A. Simon, Inorg. Chem. 45 (2006) 10786–10789.
[3] V. Smetana, V. Babizhetskyy, G.V. Vajenine, A. Simon, J. Solid State Chem. 180 (2007) 1889–1893.
[4] V. Smetana, V. Babizhetskyy, A. Simon, Z. Anorg. Allg. Chem. 634 (2008) 629–632.
[5] V. Smetana, V. Babizhetskyy, G.V. Vajenine, A. Simon, Z. Anorg. Allg. Chem. 633 (2007) 2296–2299.
[6] V. Smetana, V. Babizhetskyy, G.V. Vajenine, A. Simon, Angew. Chem. Int. Ed. 45 (2006) 6051–6053.
[7] V. Smetana, V. Babizhetskyy, C. Hoch, A. Simon, J. Solid State Chem. 180 (2007) 3302–3309.
[8] G. Cordier, M. Ludwig, D. Stahl, P. Schmidt, R. Kniep, Angew. Chem., Int. Ed. Engl. 34 (1995) 1761–1763.
[9] M. Kirchner, F. Wagner, W. Schnelle, R. Niewa, Z. Anorg. Allg. Chem. 630 (2004) 1735.
[10] M. Bailey, F. DiSalvo, J. Alloys Compd. 353 (2003) 146–152.
[11] H. Yamane, S. Sasaki, T. Kajiwara, T. Yamada, M. Shimada, Acta Crystallogr. E60 (2004) i120–i123.
[12] P. Höhn, R. Ramlau, H. Rosner, W. Schnelle, R. Kniep, Z. Anorg. Allg. Chem. 630 (2004) 1704.
[13] G. Cordier, S. Rönninger, Z. Naturforsch. 42b (1987) 825–827.
[14] A. Schlechte, Yu. Prots, R. Niewa, Z. Kristallogr.–New Cryst. Struct. 219 (2004) 349–350.
[15] M. Bailey, D. Shen, M. McGuire, D. Fredrickson, B. Toby, F. DiSalvo, H. Yamane, S. Sasaki, M. Shimada, Inorg. Chem. 44 (2005) 6680–6690.
[16] H. Pauly, A. Weiss, H. Witte, Z. Metallkunde 59 (1968) 554–558.
[17] J. Stoehr, W. Müller, H. Schäfer, Z. Naturforsch. 33b (1978) 1434–1437.
[18] S. Amerioun, U. Häussermann, Inorg. Chem. 42 (2003) 7782–7788.
[19] M. Wendorff, C. Röhr, Z. Naturforsch. 59b (2004) 619–628.
[20] G. Bruzzone, J. Less-Common Met. 11 (1966) 249–258.
[21] M. Wendorff, C. Röhr, J. Alloys Compd. 448 (2008) 128–140.
[22] M. Wendorff, C. Röhr, Z. Anorg. Allg. Chem. 631 (2005) 338–349.
[23] C. Dasarathy, Trans. Metall. Soc. AIME 245 (1969) 2015–2019.
[24] V. Smetana, A. Simon, Z. Naturforsch. 65b (2010) 643–645.
[25] A. Altomare, M. Burla, M. Camalli, B. Carroccini, G. Cascarano, C. Giacovazzo, A. Guagliardi, A. Moliterni, G. Polidori, R. Rizzi, J. Appl. Crystallogr. 32 (1999) 115.
[26] G.M. Sheldrick, in: SHELXL-97: Program for the Refinement of Crystal Structures, University of Göttingen, Germany, 1997.
[27] L. Farrugia, J. Appl. Crystallogr. 32 (1999) 837.
[28] R. Vincent, P.A. Midgley, Ultramicroscopy 53 (1994) 271–282.
[29 J. Gjonnes, V. Hansen, A. Krerneland, Microsc. Microanal. 10 (2004) 16–20.
[30] T. Weirich, J. Portillo, G. Cox, H. Hibst, S. Nicolopoulos, Ultramicroscopy 106 (2006) 164–175.
[31] M. Gemmi, X. Zou, S. Hovmoller, A. Migliori, M. Vennstrom, Y. Andersson, Acta Crystallogr. A59 (2003) 117–126.
[32] C. Own, Ph.D. thesis, Northwestern University, Evanston, Illinois, 2005.
[33] P. Jeitschko, A. Simon, R. Ramlau, Hj. Mattausch, Eur. Microsc. Microanal. 46 (1997) 21.
[34] P. Jeitschko, A. Simon, R. Ramlau, Hj. Mattausch, Z. Anorg. Allg. Chem. 623 (1997) 1447.
[35] P. Goodman, A. Moodie, Acta Crystallogr. A30 (1974) 280–290.
[36] J. Cowley, A. Moodie, Acta Crystallogr. 10 (1957) 609–619.
[37] P. Stadelmann, Ultramicroscopy 21 (1987) 131–146.
[38] Emaps 1.0, AnaliTEX 2002-2007.
[39] Crisp 2.1a, Calidris, Manhemsvägen 4, Sollentuna, Sweden, 2007.
[40] P. Blaha, K. Schwarz, G.K.H. Madsen, D. Kvasnicka, J. Luitz, WIEN2k, An Augmented Plane Wave+Local Orbitals Program for Calculating Crystal Properties (Karlheinz Schwarz, Techn. Universität Wien, Austria), 2001. 3-9501031-1-2.
[41] J.P. Perdew, S. Burke, M. Ernzerhof, Phys. Rev. Lett. 77 (1996) 3865–3868.
[42] V. Smetana, V. Babizhetskyy, C. Hoch, A. Simon, Z. Kristallogr. NCS 221 (2006) 434.
[43] D. Flot, M. Tillard-Charbonell, C. Belin, J. Am. Chem. Soc. 118 (1996) 5229–5235.
[44] B. Lee, J. Corbett, Inorg. Chem. 46 (2007) 6022–6028.
[45] V. Smetana, V. Babizhetskyy, G.V. Vajenine, C. Hoch, A. Simon, Inorg. Chem. 46 (2006) 5425–5428.
[46] L. Kienle, V. Smetana, V. Duppel, A. Simon, Z. Anorg. Allg. Chem., 636 (2010) 325–330.
[47] S. Sevov, J. Corbett, J. Solid State Chem. 103 (1993) 114–130.
[48] G.J. Snyder, A. Simon, Dalton Trans. (1994) 1159–1160.
[49] A. Westgren, Jernkontor. Ann. 111 (1933) 525–530.